[7]F. Kh. Gel'mukhanov and A. M. Shalagin, Zh. Eksp. Teor. Fiz. **78**, 1674 (1980) [Sov. Phys. JETP **51**, 839 (1980)].
[8]A. M. Dykhne and A. N. Starostin, Zh. Eksp. Teor. Fiz. **79**, 1211 (1980) [Sov. Phys. JETP **52**, 612 (1980)].
[9]D. J. Ehrlich, R. M. Osgood Jr, and T. F. Deutsch, Appl. Phys. Lett. **36**, 698 (1980).
[10]R. W. Haynes, G. M. Metze, V. G. Kreismanis, and L. F. Eastman, Appl. Phys. Lett. **37**, 344 (1980).
[11]D. J. Ehrlich, R. M. Osgood Jr, and T. F. Deutsch, Digest of Papers presented at Eleventh Intern. Conf. on Quantum Electronics, Boston, Mass., 1980, publ. by Optical Society of America, Washington, D.C. (1980), Paper C9, p. 588.
[12]F. Kh. Gel'mukhanov and A. M. Shalagin, Preprint No. 133 [in Russian], Institute of Automation and Electrometry, Siberian Branch of the Academy of Sciences of the USSR, Novosibirsk (1980).

Translated by R. M. Durham

Optical breakdown of molecular nitrogen in a wide range of pressures near a solid target

V. I. Mazhukin, A. A. Uglov, and B. N. Chetverushkin

A. A. Baĭkov Institute of Metallurgy, Academy of Sciences of the USSR, Moscow
(Submitted May 5, 1981)
Kvantovaya Elektron. (Moscow) **9**, 906–917 (May 1982)

An investigation was made of the conditions for the formation and evolution of a laser plasma near a metal surface in nitrogen at pressures of 1–140 atm. A neodymium laser ($\lambda = 1.06\,\mu$) operating in the spiky regime with an average power density $G = 1$–10 MW/cm^2 was used in the experiments. A numerical analysis was made of the characteristics of optical breakdown of molecular nitrogen in the pressure range 10–200 atm. The experimental data were interpreted on the basis of the results of numerical modeling.

PACS numbers: 52.50.Jm, 52.40.Hf, 42.60.He

1. INTRODUCTION

A low-temperature laser plasma is generally used for applications in modern engineering and technology at pressures of the surrounding gaseous medium generally not exceeding 1 atm. Experiments[1,2] on a laser plasma formed near metal surfaces at high ambient pressures showed that, under these conditions, the plasma has many interesting characteristics and may be used to harden materials.[1,3,4] In this context, a detailed analysis of the main laws governing the evolution of a laser plasma is of considerable topical interest. Of particular interest are the initial stages of evolution, especially the optical breakdown stage of the gas, which determine the subsequent character of the interaction between the radiation and the material.

Optical breakdown of gases has been the subject of comprehensive investigations for a long time. It should be noted that laser-induced breakdown of gases is characterized by many short-lived interdependent and interrelated processes, giving rise to major difficulties when this phenomenon is studied.[5,6]

It has been established experimentally that breakdown has a threshold both in terms of intensity and gas pressure.[7] Moreover, the evolution of breakdown is also strongly influenced by external electric and magnetic fields[8,9] and also by the parameters of the laser system such as the frequency and pulse duration,[10] the radius of the focusing spot,[11] the type of gas and whether it contains impurities and particles.[12,13]

Ideas on two mechanisms for optical breakdown have now been put forward. One of these is based on multiphoton ionization.[14] The other mechanism proposed by Zel'dovich and Raizer[15] is based on the growth of an electron avalanche. Depending on the spectral range and intensity of the optical radiation, one of the following mechanisms predominates: avalanche ionization in dense gases ($p \geq 1$ atm) at low laser radiation densities (~1 GW/cm^2) or multiphoton ionization predominates at low pressures ($p \ll 1$ atm) and high radiation intensities (~100 GW/cm^2). There are also many complex phenomena where both mechanisms are observed simultaneously or one after the other.[5]

When a solid target is placed in the focal plane, this sharply reduces the threshold values of the radiation intensity[16,17] since interaction between laser radiation and a condensed medium, which is characterized by a wide variety of effects, gives rise to many factors promoting breakdown and facilitating its evolution. These factors include vaporization of the target material,[17,18] thermionic emission of electrons and ions,[19,20] shock wave generation accompanying intensive vaporization and mechanical damage to the surface,[21,22] and other factors.

 0049-1748/82/050573-08$04.10 © 1982 American Institute of Physics

Under almost all conditions, optical breakdown of gases is characterized by high concentrations of chemically active particles, excited atoms and molecules, ions, and so on, and most collisional reactions take place under highly nonequilibrium conditions. The relationship between the chemical kinetic characteristics and the hydrodynamic and transport parameters may then be extremely complex. As a result, too much reliance should not be placed on extremely simplified models and approximate calculations.

A more accurate method of investigating these systems involves making realistic allowance for all the difficulties by developing fairly comprehensive mathematical models and then solving these numerically on a computer.

Bearing in mind that breakdown of a gas followed by the growth of plasma formations under the influence of laser radiation is a continuous process and also bearing in mind the real capabilities of existing computers, it is advisable to divide the process of studying the evolution of a laser plasma into three arbitrary stages. The first stage involves analyzing the breakdown of a cold gas by laser radiation at the level of the elementary reactions. Chemical kinetics and transport processes are analyzed at this stage. No hydrodynamic processes take place since the gas temperature is still low.

The second stage involves the formation of a plasma jet (cloud) which is barely transparent to laser radiation. Allowance is made for the initial stage of gasdynamic evolution of the plasma. In many cases, depending on the pressure and intensity, collisional reactions are neglected.

The third stage involves the quasisteady-state propagation of plasma discharges and it was investigated in Refs. 5 and 6.

Using experimental data and numerical modeling methods, the present paper investigates the processes during the first stage of plasma evolution: breakdown of molecular nitrogen near a molybdenum surface by $\lambda = 1.06$ μ laser radiation in a wide range of pressures $p = 10$–200 atm at low laser radiation power densities $G_0 = 10^7$–10^9 W/cm^2. In this case, particular attention is paid to numerical modeling of the process.

2. EXPERIMENT

A neodymium laser ($\lambda = 1.06$ μ) operated in the spiky regime with a pulse duration $\tau_i \approx 0.5$–0.8 msec and an energy of up to 50 J was used in the experiments. The average radiation intensity per pulse G_0 in a focal spot of radius $r_f \approx 250$–300 on the surface of the target was ~10 MW/cm^2. In individual spikes of ~1 μsec duration the power density exceeded $G_0 \approx 100$ MW/cm^2.

The apparatus was described in Ref. 1. Laser radiation was fed into a high-pressure chamber filled with nitrogen containing the following impurities: $O_2 \leq 10^{-3}$%, moisture ≤ 5 mg/cm^3, $H_2 \leq 10^{-3}$%, and total carbon-containing impurities less than 10^{-3}%. Before the experiment, the chamber was repeatedly scrubbed with nitrogen. The radiation was focused by means of a lens situated inside the chamber onto a molybdenum plate ~2 mm thick. Processes taking place inside the chamber were recorded using an SFR-1 high-speed image converter camera operating in the framing mode.

The experimental data showed that the interaction between the laser radiation and the target depended strongly on the nitrogen pressure in the chamber. A severalfold increase in the contamination of the gas compared with the initial value had no significant influence on the reproducibility of the effects observed. The experiments were carried out five or six times at each pressure.

When the molybdenum target was irradiated at a nitrogen pressure of 1 atm, a through hole ~0.8 mm in diameter was formed in the plate. The jet of the ejected material had a low luminosity, its diameter was small, and its length was ~1.6 cm.

When the pressure was increased to 10 atm, a smaller-diameter (~0.5 mm) through hole was drilled in the target. A "halo" of crystallized metal was observed on the surface of the plate around the edges of the hole. An image converter photograph of the process showed that intensive vaporization of material took place from the target surface. Approximately 0.3 msec after the beginning of the pulse, breakdown occurred in the target vapor and the brightness of the jet reached its maximum. The size of the zone of thermal interaction around the hole in the plate was ~1.4 mm.

When the pressure was increased to 30 atm, ejection of target material decreased appreciably. A shallow crater was formed in the target rather than a through hole. The velocity of the plasma front was ~10 m/sec. The jet was approximately cylindrical with a maximum diameter of ~0.6 and a height of ~1 mm. The plasma jet was formed above the surface within approximately 0.1 msec.

When the nitrogen pressure was increased to 50 atm, a black interaction zone with a fused region at the center was formed on the surface of the target. Negligible ejection of material occurred and the diameter of the interaction zone was ~0.5 mm. A plasma jet having clearly defined boundaries and a highly luminous region at its front was formed above the surface.

In the pressure range 60–90 atm, negligible fusion occurred and the diameter of the interaction zone was 0.4–0.5 mm. As the nitrogen pressure increased, the plasma jet became spheroidal. Formation of the plasma jet took place approximately 30–50 μsec after the beginning of irradiation.

At pressures higher than 100 atm, there were almost no traces of fusion. The thermal interaction zone differed in color from the rest of the surface and its diameter was ~0.3 mm. The luminosity of the plasma front was extremely high compared with the rest of the cloud. Within 200 μsec the brightest region had shifted to the center of the jet and by the end of the pulse, its luminosity was higher than that at the periphery. The propagation velocity of the plasma front was ~5 m/sec.

These experiments demonstrated that at pressures higher than 60 atm a plasma forms under conditions such that vaporization processes are strongly suppressed and the molybdenum vapor cannot play a decisive role in the gas breakdown mechanism.

3. THEORETICAL ANALYSIS AND DISCUSSION OF RESULTS

A physical model of breakdown will be used as the basis of a mechanism for thermionic emission of electrons from the surface of a molybdenum target and evolution of an electron–ion avalanche in a dense gas under the influence of laser radiation. The high pressure of the surrounding medium decreases electron diffusion and "shifts" the boiling point of the metal toward higher values. As a result, at high pressures the surface of a target heated to high temperatures is not damaged but a fairly high electron density is found near the surface, its value being governed by the emission properties of the target and by the space charge potential. On entering the gas, the thermonic electrons acquire the energy needed to ionize the neutral particles as a result of bremsstrahlung absorption of laser radiation in the field of the ions and neutrals. Subsequently, evolution of the avalanche takes place in accordance with classical concepts.[15]

The first attempts at numerical modeling using the proposed physical model[23] showed that, in principle, it should be possible for an avalanche to develop at pressures higher than 100 atm and laser radiation intensities higher than 100 MW/cm^2.

We shall make a numerical analysis of the conditions and characteristics of the evolution of optical breakdown in molecular nitrogen over a wide range of pressures and, by comparing the results with the experimental data, we shall determine the range of validity of the proposed physicochemical and mathematical models.

The evolution of an electron avalanche in molecular gases is characterized by complex collisional reaction kinetics. The present model considers chemical kinetics and transport processes taking place simultaneously in the atomic and molecular components of the gas.

Allowance was made for the following reactions taking place in nitrogen: electronic excitation and electron-impact deexcitation of atoms and molecules, $N + e \rightleftharpoons N^* + e$, $N_2 + e \rightleftharpoons N_2^* + e$, electron-impact vibrational excitation of molecules, $N_2 + e \rightarrow N_2^{\times} + e$, thermal dissociation and electron-impact dissociation $N_2 + N_2 \rightarrow 2N + N_2$, $N_2 + e \rightarrow 2N + e$, association reactions $N_2 + 2N \rightarrow N_2^{\times} + N_2$, $N + 2N \rightarrow N_2^{\times} + N$, ionization of atoms and molecules from the ground and excited states and three-body recombination $N + e \rightleftharpoons N^+ + 2e$, $N^* + e \rightleftharpoons N^+ + 2e$, $N_2 + e \rightleftharpoons N_2^+ + 2e$, $N_2^* + e \rightleftharpoons N_2^+ + 2e$, associative ionization of atoms $N + N \rightarrow N_2^+ + e$, and dissociative recombination $N_2^+ + e \rightarrow 2N$, $N_3^+ + e \rightarrow 3N$, $N_4^+ + e \rightarrow 2N_2$. Of the various transport processes, allowance was made for diffusion and drift in the space charge field of the charged particles N_e, N_i^+ (the expressions for J_i^+ and J_e), and for the thermal conductivity of the electron gas and heavy particles described by the diffusion terms $(\partial/\partial x)\varkappa_e(\partial T_e/\partial x)$ and $(\partial/\partial x)\varkappa_g(\partial T_g/\partial x)$.

These reactions are described by the chemical kinetics Eqs. (1)–(9) (see below). A more detailed description of collisional reactions and their rate constants was given in Ref. 24. An analysis of collisional reactions showed that the rate constants are functions of three temperatures: the translational temperatures of the electrons T_e and heavy particles T_g, and the vibrational temperature of the molecules T_v. Thus, the system of kinetic equations is supplemented by three energy balance equations (10)–(12). Allowance for inelastic electron energy losses in the molecular component of the gas was made using the experimental coefficient $\delta(\mathscr{E})$ (Ref. 25), which is the factor by which the total electron energy losses as a result of inelastic collisions exceed those due to elastic collisions. The space charge field is described by the Poisson equation (13).

The mathematical formulation of the problem in the one-dimensional three-temperature approximation finally takes the form

$$\frac{\partial N_2}{\partial t} = -(k_2^- N_2 - \beta_2^+ N_2^+ N_e) N_e - (k_2^* N_2 - \beta_2^* N_2^*) N_e - (k_4^c N_2^+ N_2 - \beta_4^c N_4^+) N_2 - (k_3^c N^+ N_2 - \beta_3^c N_3^+) N_2 - k_d^e N_2 N_e - (k_d N_2 - k_a N^2) N_2 + k_a^a N^3 + 2\alpha_4 N_4^+ N_e; \quad (1)$$

$$\frac{\partial N_2^*}{\partial t} = (k_2^* N_2 - \beta_2^* N_2^*) N_e - (k_2^{*-} N_2^* - \beta_2^+ N_2^+ N_e) N_e - k_d N_2^* N_e; \quad (2)$$

$$\frac{\partial N_2^+}{\partial t} = (k_2^+ N_2 - \beta_2^+ N_2^+ N_e) N_e + (k_2^{*+} N_2^* - \beta_2^+ N_2^+ N_e) N_e - (k_4^c N_2^+ N_2 - \beta_4^c N_4^+) N_2 - \alpha_2 N_2^+ N_e + k_a N N - \frac{\partial j_2^+}{\partial x}; \quad (3)$$

$$\frac{\partial N_4^+}{\partial x} = (k_4^c N_2^+ N_2 - \beta_4^c N_4^+) N_2 - \alpha_4 N_4^+ N_e - \frac{\partial j_4^+}{\partial x}; \quad (4)$$

$$\frac{\partial N}{\partial t} = k_d^e N_2 N_e + (k_d (N_2 + N_2^*) - k_a N^2) N^2 - k_a^a N^3 - (k^+ N - \beta^+ N^+ N_e) \times N_e - (k^* N - \beta^* N^*) N_e - k_a N N + 2\alpha_2 N_2^+ N_e + 3\alpha_3 N_3^+ N_e; \quad (5)$$

$$\frac{\partial N^*}{\partial t} = (k^* N - \beta^* N^*) N_e - (k^{*+} N^* - \beta^+ N^+ N_e) N_e; \quad (6)$$

$$\frac{\partial N^+}{\partial t} = (k^+ N - \beta^+ N^+ N_e) N_e + (k^{*+} N^* - \beta^+ N^+ N_e) N_e - (k_3^c N^+ N_2 - \beta_3^c N_3^+) N_2 - \frac{\partial J^+}{\partial x}; \quad (7)$$

$$\frac{\partial N_3^+}{\partial t} = (k_3^c N^+ N_2 - \beta_3^c N_3^+) N_2 - \alpha_3 N_3^+ N_e - \frac{\partial j_3^+}{\partial x}; \quad (8)$$

$$\frac{\partial N_e}{\partial t} = (k_2^+ N_2 - \beta_2^+ N_2^+ N_e) N_e + (k_2^{*+} N_2^* - \beta_2^+ N_2^+ N_e) N_e + (k^+ N - \beta^+ N^+ N_e) N_e^+ + (k^{*+} N^* - \beta^+ N^+ N_e) N_e + (k_a N N - \alpha_2 N_2^+ N_e) - \alpha_3 N_3^+ N_e - \alpha_4 N_4^+ N_e - \frac{\partial j_e}{\partial x}; \quad (9)$$

$$\frac{3}{2}\frac{\partial}{\partial t}(N_e T_e) = \left(\frac{4\pi e^2 G}{mc(\omega^2 + \nu_{\text{eff}}^2)} - \frac{3}{2}\delta\lambda(T_e - T_g)\right)(\nu_{ei} + \nu_{en}) N_e + \left(\frac{4\pi e^2 G}{mc(\omega^2 + \nu_{\text{eff}}^2)} - 3\lambda(T_e - T_g)\right)(\nu_{ei}^a + \nu_{en}^a) N_e - I^+ (k^+ N - \beta^+ N^+ N_e) N_e - I^* (k^* N - \beta^* N^*) N_e - I^{*+} (k^{*+} N^* - \beta^+ N^+ N_e) N_e + \frac{\partial}{\partial x}\varkappa_e \frac{\partial}{\partial x} T_e; \quad (10)$$

$$\frac{\partial}{\partial t}(N_g T_g) = \lambda(T_e - T_g)(\nu_{ei} + \nu_{en}) N_e + 2\lambda(T_e - T_g)(\nu_{ei}^a + \nu_{en}^a) N_e + T_g((k_4^c N_2^+ N_2 - \beta_4^c N_4^+) N_2 + (k_3^c N^+ N_2 - \beta_3^c N_3^+) N_2) + \frac{\partial}{\partial x}\varkappa_g \frac{\partial}{\partial x} T_g; \quad (11)$$

$$\frac{\partial}{\partial t}(N_2 T_v) = \hbar\omega_v k^{\times} N_2 N_e - I_d((k_d N_2 - k_a N^2) N_2 - k_a^a N^3); \quad (12)$$

$$\frac{\partial^2 U}{\partial x^2} = -\frac{e}{\xi}\left(N_e - \sum_{i=1}^{4} N_i^+\right); \quad E = -\operatorname{grad} U; \quad (13)$$

$$\vec{J}_e = e\mu_e N_e E + eD_e \operatorname{grad} N_e;$$
$$\vec{J}_i^+ = e\mu_i N_i^+ E - eD_i \operatorname{grad} N_i^+;$$
$$\lambda = m/M; \quad N_g = (N + N^* + N_2 + N_2^* + N^+ + N_2^+ + N_3^+ + N_4^+);$$
$$\nu_{\text{eff}} = (\nu_{en} + \nu_{ei}); \quad \beta^{*+} = \beta^+.$$

The surface temperature and the thermal electron flux were defined at the left-hand boundary $x = 0$:

$$D_e \frac{\partial N_e}{\partial x} = BT^2 \exp\left(-\frac{\varphi + \varphi_1}{T}\right), \quad \sum_{i=1}^{4} N_i^+ = 0,$$

$$T = \frac{2G_n}{\lambda}\left(\frac{at}{\pi}\right)^{1/2}, \quad U = 0.$$

At the right-hand boundary $x = L$, the boundary conditions were defined in the form of relationships linking the fluxes and their functions:

$$D_e \frac{\partial N_e}{\partial x} = -\frac{1}{2} v_e N_e, \quad D_i \frac{\partial N_i^+}{\partial x} = -\frac{1}{2} v_g N_i^+,$$

$$\varkappa_e \frac{\partial T_e}{\partial x} = -\frac{1}{2} v_e N_e T_e, \quad \varkappa_g \frac{\partial T_g}{\partial x} = -\frac{1}{2} v_g N_g T_g,$$

when $U = 0$. The following notation is used: N, N^*, N_2, N_2^*, $N_2^\times$, N^+, N_2^+, N_3^+, N_4^+, and N_e are the charged and neutral particle densities; k and α are the rate constants of the direct reactions; β are the rate constants of the reverse reactions; $\omega = 2\pi\nu$ is the laser radiation frequency; G_n is the fraction of the laser radiation absorbed by the surface; $G = (1 + R)G_0$; v_e and v_g are the thermal velocities of the electrons and heavy particles; ν_{en}^a, ν_{ei}^a, ν_{en}, and ν_{ei} are the frequencies of collisions between atomic ions or neutrals (index a) and molecular ions or neutrals with electrons; D_e, D_i, μ_i, and μ_e are the electron and ion diffusion coefficients and mobilities; $\varkappa_e$ and $\varkappa_g$ are the thermal conductivities of the electrons and heavy particles; a and λ are the thermal diffusivity and thermal conductivity of molybdenum; φ is the work function; $\varphi_1 = eU$ is the additional work function produced by the space-charge field; U and E are the potential and intensity of the electric field; $R = 0.2$ is the reflection coefficient.

The procedure described in Ref. 26 was used to obtain a numerical solution of the system (1)–(13). Optical breakdown was modeled numerically in the pressure range 10–200 atm for a laser radiation intensity $G_0 = 0.9$ GW/cm^2.

We shall analyze a general system for the evolution of breakdown at a nitrogen pressure of 100 atm (Figs. 1 and 2).

Optical breakdown is taken to be that state of a material when the electron temperature T_e increases sharply in a certain local region, causing avalanche-like ionization and, as a result, an increase in the temperature of the heavy particles T_g. A local region of intensive laser radiation absorption is formed.

Under normal conditions, nitrogen is transparent to laser radiation with the quantum energy $h\nu = 1.17$ eV and the total flux is incident on the target surface from the right. In this case, some of the flux RG_0 is reflected and the rest $G_n = (1 - R)G_0$ is absorbed. Thermionic emission is initiated from the surface of the target. In elastic collisions with gas molecules over the time $t \approx 0.2$ nsec the electrons acquire the energy $T_e = 1.1$ eV in the laser radiation field. Under the influence of

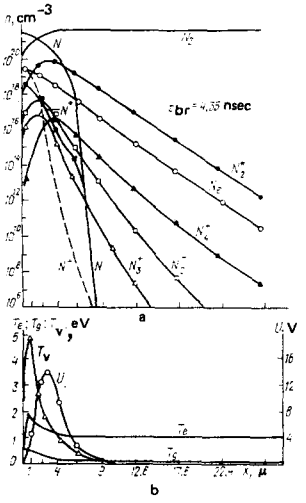

FIG. 1.

thermionic emission, a space charge is formed near the surface, its potential U impeding electron emission by generating the additional work function φ_1. When the space charge potential reaches $U \approx 3$ V ($t \approx 2$ nsec), electron emission from the surface ceases. The electron density in the region $x \leq 0.4$ μ reaches $N_e \approx 2 \times 10^{18}$ cm^{-3} and the surface temperature is 0.34 eV. This spatial distribution of N_e may be considered to be the initial electron density. In spite of this high electron density, breakdown of the gas does not occur in this time interval. All the phenomena in the radiation zone are governed by collisions in the molecular component of the gas. Ionization of the molecules takes place comparatively slowly as a result of the insufficiently high electron energy, which is limited by inelastic losses the coefficient $\delta(T_e)$ decreases rapidly with increasing temperature. The atomic density is still low due to the low vibrational temperature $T_v \sim 0.3$ eV (see Fig. 2), which determines the degree of thermal dissociation (the rate constant k_d is a function of the vibrational temperature[24]).

The main dissociation mechanism at vibrational temperatures $T_v < 0.6$ eV is electron impact dissociation.

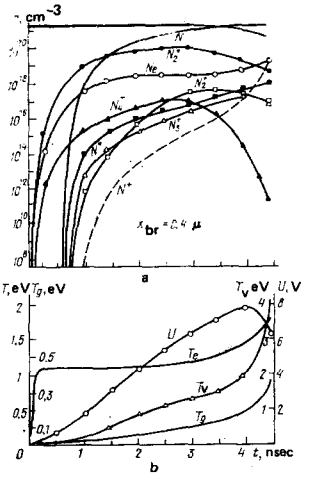

FIG. 2.

It has been established[27] that the transfer of electron energy to the vibrational degrees of freedom in molecular nitrogen is extremely rapid. As a result, the energy acquired by the electrons in the laser radiation field is mainly dissipated in vibrational excitation of the molecules. Since the reverse process of deexcitation is negligible in the nanosecond range and, in addition, the vibrational energy is further supplemented by the thermal association reactions $N_2 + 2N \rightarrow N_2^x + N_2$, $N + 2N \rightarrow N_2^x + N$, the vibrational temperature may exceed the electron temperature in a certain time interval.

By the time $t \approx 3$ nsec, the value of T_v at the point $x = 0.4$ μ reaches 3 eV ($T_e = 1.2$ eV, see Fig. 2). Vigorous thermal dissociation of the gas takes place, reaching ~90% at $t \approx 4$ nsec (see Figs. 1 and 2). At this point, collisional processes in the atomic component of the gas become a decisive factor. The electron temperature at the point $x = 0.4$ μ is governed by electron–neutral and electron–ion collisions in the atomic gas. An increase in the ion densities N^+ and N_3^+ increases the collision frequency ν_{ei}^a and when the frequencies $\nu_{ei}^a \sim \nu_{en}^a$ become equal, the temperature T_e increases, intensifying the ionization process and also causing a further increase in ν_{ei}^a and T_e, i.e., evolution of an electron–ion avalanche is initiated. The ion density N^+ increases and becomes equal to the electron density N_e, which decreases the potential U in this region. The electric field becomes self-consistent and the diffusion becomes ambipolar.

The end of the breakdown stage is determined by the attainment of the maximum electron temperature at the breakdown point. The temperature T_e reaches its maximum $T_{e\max} = 1.79$ eV at the point $x = 0.4$ μ at the time $t = 4.35$ nsec when $N_e \sim N^+ = 3 \times 10^{19}$ cm^{-3} and $T_v \approx 4.5$ eV. Subsequently, under the influence of diffusion, the breakdown zone is shifted to the right, in the opposite direction to the laser radiation. An increase in the electron density N_e promotes more efficient energy transfer to the translational degrees of freedom of the gas. The temperature T_g increases to 0.4 eV in the breakdown zone; at this point the calculations were terminated since it was then necessary to allow for gasdynamic expansion of the gas, i.e., to study the next stage of evolution of the laser plasma.

During breakdown the temperature of the surface reaches 0.45 eV which is close to the boiling point of molybdenum at a pressure of 1 atm. This suggests that at pressures of 100 atm no strong vaporization processes will occur.

Calculations made to determine the threshold radiation intensity needed for breakdown showed that it lies in the range $G_0 = 0.4$–0.5 GW/cm^2. At lower values of G_0 the average electron energy does not rise above 0.7 eV, which is insufficient both for multistage ionization and for efficient excitation of vibrational states responsible for thermal dissociation.

Under these conditions, molybdenum vapor cannot have a decisive influence on the process. This is confirmed by estimates of the condition which must be satisfied for the evolution of an electron avalanche (ionization from the ground state)[17]:

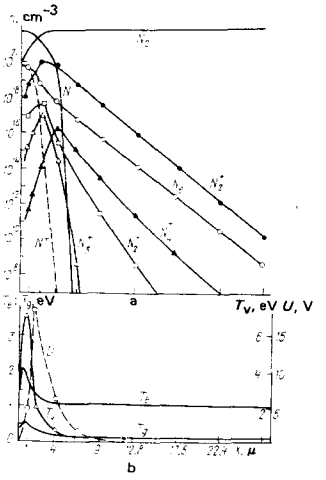

FIG. 3.

$$\frac{d\mathscr{E}}{dt} = \frac{4\pi e^2 G_0}{mc\omega^2}\nu_{\text{eff}} > \left(\frac{d\mathscr{E}}{dt}\right)_{\text{th}}^{\max} = \frac{2m}{M}\nu_{\text{eff}} G_0,$$

where $(d\mathscr{E}/dt)_{\text{th}}^{\max}$ is the maximum rate of energy losses as a result of elastic collisions.

From this condition the threshold radiation intensity for molybdenum is $G_0 > 6 \times 10^9 I/\lambda A > 0.4$ GW/cm^2; $A = 95.95$; $I = 7.1$ eV; $\lambda = 1.06$ μ.

Thus, the laser power density needed for the evolution of an avalanche in molybdenum vapor is approximately the same as that for nitrogen at a pressure of 100 atm although the vaporization processes develop considerably later than thermionic emission. Thus, the presence of molybdenum vapor at high pressures can only intensify an avalanche process already initiated in nitrogen but cannot cause it.

For comparison with the experimental data, breakdown was modeled numerically for various pressures (Figs. 3–5).

Figure 3 shows the spatial distributions of the fundamental particle densities, temperatures, and the electric field potential at a pressure of 200 atm. It can be seen that the breakdown zone is compressed ($x_{\text{br}} = 0.25$ μ), the maximum electron temperature is increased

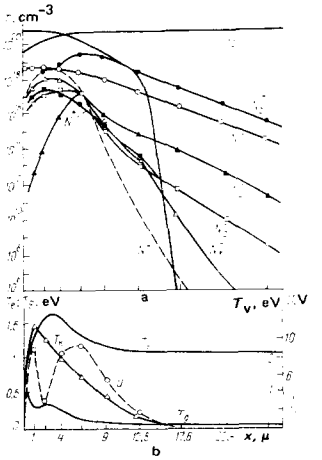

FIG. 4.

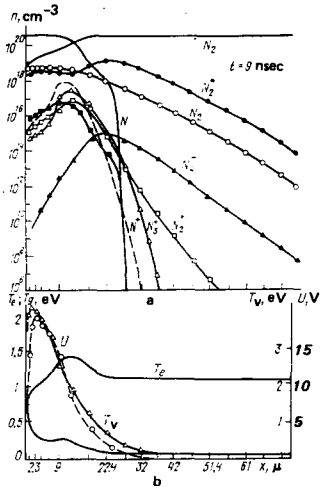

FIG. 5.

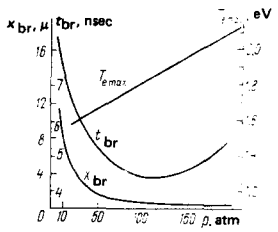

FIG. 6.

(T_e = 2.1 eV), and the breakdown time is also increased (t_{br} = 5.6 nsec).

When the pressure is decreased to 30 atm (Fig. 4), the breakdown point becomes further from the surface x_{br} = 4 μ as a result of the increased role of diffusion processes, and the maximum electron temperature decreases T_{emax} = 1.6 eV as a result of a decrease in the collision frequency ν_{ei}^a. The breakdown time is t_{br} = 6.1 nsec.

When the pressure is reduced to 10 atm, no clearly defined breakdown zone is observed (Fig. 5). Although the electron temperature is slightly increased in the region $x \sim 12$–15 μ, ($T_{emax} \approx 1.4$ eV), this is insufficient for the growth of an avalanche. As a result of the high diffusion losses, the condition $\nu_{ei}^a > \nu_{en}^a$ is not satisfied. The maximum ion density $\sum_1^4 N_i^+ \approx 7 \times 10^{17}$ cm^{-3} is appreciably lower than the electron density $N_e \sim 5 \times 10^{18}$ cm^{-3}. On the other hand, the surface temperature increases to 0.7–0.8 eV[1)] and this evidently causes intensive vaporization of the target material.

Thus, optical breakdown of molecular nitrogen due to thermionic emission phenomena may be expected at pressures $p \geq 30$ atm. At lower pressures, for example, at 10 atm, the breakdown time increases appreciably and this increases the possibility of vaporization products being formed in the irradiated zone. Moreover, the threshold intensity needed for breakdown of nitrogen exceeds $G_0 \sim 1$ GW/cm² which is substantially higher than the threshold values for breakdown of molybdenum vapor. These results are readily confirmed by the experimental observations.

Damage to the surface of the target observed experimentally at p = 30–50 atm does not eliminate the possibility of breakdown in nitrogen, since this damage may be due to the thermal regime of the plate at the later gasdynamic stage of evolution of the plasma near the surface.

Experimental investigations of optical breakdown in pure nitrogen in the absence of a target[7] showed that the pressure dependence of the threshold radiation intensity $G_{br}(p)$ has a clearly defined extreme character with a minimum at 102 atm.

Figure 6 shows dependences of the breakdown time t_{br}, the distance from the target surface to the breakdown zone x_{br}, and the maximum electron temperature T_{emax} on the pressure p for a constant layer radiation power density $G_0 \approx 0.9$ GW/cm². The curve $t_{br}(p)$ shows good qualitative agreement with the experimental curve $G_{br}(p)$ (Ref. 7), and has the same extreme behavior with a minimum near 100 atm, i.e., for a constant value of G_0 the most favorable conditions for breakdown are found near 100 atm. As the pressure decreases, the role of diffusion processes increases, the electron–neutral collision frequencies ν_{en}^a and ν_{en} decrease, and the electrons have to cover a substantially greater diffusion path before they acquire an energy of the order of 1 eV and the condition $\nu_{ei}^a \geq \nu_{en}^a$ is satisfied. Thus, the breakdown time and the distance from the breakdown zone increase and the maximum electron temperature decreases.

As the pressure increases, the collision frequencies increase, energy is acquired more rapidly by the electrons, and their diffusion path becomes shorter. As a result, T_{emax} increases and the breakdown time and distance from the breakdown zone decrease.

However, if the pressure is too high ($p > 100$ atm), the breakdown time increases as a result of the deteriorating conditions for acquisition of energy by the electrons at the initial stage of evolution of the avalanche (the condition $\omega^2 \gg \nu_{eff}^2$ becomes $\omega^2 > \nu_{eff}^2$), when electron–neutral collisions predominate ($\nu_{en}^a > \nu_{ei}^a$), and also since it is more difficult for the breakdown condition $\nu_{ei}^a > \nu_a^{en}$ ($N_{e,i}^+ \sim 0.008N$) to be satisfied because a larger number of neutral particles must be ionized; this requires a longer time, exactly as for the evolution of breakdown after the attainment of the maximum temperature T_{emax}.

Attention is drawn to the monotonic increase in the curve $T_{emax}(p)$ which suggests that at pressures higher than 100 atm, the condition for acquisition of energy by the electrons as a whole does not deteriorate. From this it can be concluded that optical breakdown in nitrogen at pressures $p > 100$ atm can always be observed for a value of G_0 corresponding to the minimum of the curve $G_{br}(p)$ if the laser pulse duration is not limited.

We shall estimate the role of various reactions in the evolution of breakdown.

Calculations showed that the most important reactions for the initiation of breakdown in nitrogen are vibrational excitation, dissociation, and multistage ionization.

Conversion reactions cease to be important at $T_g \sim 0.2$ eV. Dissociative recombination processes involving molecular ions and clusters play an important role in the molecular component of the gas, determining the particle densities N_2^+, N_3^+, and N_4^+. As a result of their high rates (the rate constants are of the order of 10^{-6}–10^{-8} cm^3/sec), these reactions limit the evolution of breakdown in the molecular component of the gas.

Under the conditions of the problem with an electron source, reactions involving ionization of atoms and molecules from the ground state make no appreciable contribution and may be neglected.

We shall discuss in greater detail the role of associative ionization of atoms $N + N \to N_2^+ + e$. In Refs. 28 and 29 it was postulated that under conditions similar to those studied, associative ionization plays an extremely important role and is the main breakdown mechanism. In these investigations it is assumed that in a gas heated by the surface of the target to a temperature of 0.4 eV, the number of charged particles formed as a result of associative ionization is sufficient for a process similar to a thermal explosion to take place in the gas. We shall give the rate equation for the $N + N \rightleftharpoons N_2^+ + e$ reaction:

$$dN_2^+/dt = k_\alpha NN - \alpha_2 N_2^+ N_e.$$

From Refs. 30 and 31 we have $k_\alpha = 2.7 \times 10^{-11} \exp(-5.4/T_g)$ cm^3/sec and $\alpha_2|_{T_g=0.4\text{ eV}} \approx 10^{-8}$ cm^3/sec.

Assuming that $N_2^+ \sim N_e$, we shall use the steady-state solution of the equation $dN_2^+/dt = 0$ to determine the maximum value of the function $N_2^+ \approx 10^8$ cm^{-3}. This charged particle density is insufficient for the growth of an avalanche or for the initiation of processes similar to a thermal explosion since under these conditions, the gas is completely transparent to laser radiation.

Associative ionization can evidently play an appreciable role under conditions when the gas temperature is high ($T_g \geq 1$ eV) and there are few free electrons. Under the conditions of the problem with an electron source, associative ionization can be neglected.

We note the main features of breakdown of a dense molecular gas by laser radiation.

a. Optical breakdown in molecular nitrogen develops under conditions when the gas is almost completely converted to the atomic state. This means that the mathematical model (1)–(13) can be used as a standard for rougher approximations. Using only kinetic equations for the atomic component for numerical modeling[26] gives qualitatively correct results.

b. The characteristic breakdown times and threshold laser radiation densities can be used to interpret breakdown observed experimentally as breakdown in a laser radiation spike.

c. At high pressures a metal target functions as an electron source. From this it follows that the breakdown process is relatively insensitive to the presence of impurities since their contribution is appreciably smaller.

d. Electron and heavy particle heat conduction processes only play a part at the initial stage of establishment of the temperatures T_g and T_e.

e. The electric fields induced by the space charge are weak, i.e., they do not cause distortions of the Maxwellian distribution function and thus they need not always be taken into account.

f. The condition for the appearance of an avalanche is that the Coulomb collision frequency should predominate over the electron–neutral collision frequency and this is reliably satisfied when $\sum_{i=1}^{4} N_i^+ \approx 0.008(N + N^* + N_2 + N_2^*)$.

[1)]The model (1)–(13) neglects phase transitions in the molybdenum target so that the real temperature of the target is lower.

[1]N. N. Rykalin, A. A. Uglov, and M. M. Nizametdinov, Zh. Eksp. Teor. Fiz. **69**, 722 (1975) [Sov. Phys. JETP **42**, 367 (1975)].
[2]N. N. Rykalin, A. A. Uglov, and M. M. Nizametdinov, Dokl. Akad. Nauk SSSR **218**, 330 (1974) [Sov. Phys. Dokl. **19**, 599 (1975)].
[3]A. A. Uglov and M. M. Nizametdinov, Fiz. Khim. Obrab. Mater. No. 2, 133 (1977).
[4]A. L. Galiev, L. L. Krapivin, L. I. Mirkin, and A. A. Uglov, Dokl. Akad. Nauk SSSR **251**, 336 (1980) [Sov. Phys. Dokl. **25**, 208 (1980)].
[5]Yu. P. Raizer, Laser-Induced Discharge Phenomena, Consultants Bureau, New York (1977).
[6]Yu. P. Raĭzer, Principles of Modern Physics of Gas-Discharge Processes [in Russian], Nauka, Moscow (1980).
[7]D. H. Gill and A. A. Dougal, Phys. Rev. Lett. **15**, 845 (1965).
[8]A. P. Darmanyan, V. E. Mitsuk, and V. A. Chernikov, Pis'ma Zh. Eksp. Teor. Fiz. **8**, 117 (1968) [JETP Lett. **8**, 71 (1968)].
[9]L. E. Vardzigulova, S. D. Kaĭtmazov, and A. M. Prokhorov, Pis'ma Zh. Eksp. Teor. Fiz. **6**, 799 (1967) [JETP Lett. **6**, 253 (1967)].
[10]H. T. Buscher, R. G. Tomlinson, and E. K. Damon, Phys. Rev. Lett. **15**, 847 (1965).
[11]R. W. Minck and W. G. Rado, Physics of Quantum Electronics, (Proc. Intern. Conf., San Juan, Puerto Rico, 1965), McGraw-Hill, New York (1966), p. 527.
[12]V. E. Mitsuk, V. I. Savoskin, and V. A. Chernikov, Pis'ma Zh. Eksp. Teor. Fiz. **4**, 129 (1966) [JETP Lett. **4**, 88 (1966)].
[13]F. V. Bunkin and V. V. Savranskiĭ, Zh. Eksp. Teor. Fiz. **65**, 2184 (1973) [Sov. Phys. JETP **38**, 1091 (1974)].
[14]A. H. Gold and H. B. Bebb, Phys. Rev. Lett. **14**, 60 (1965).
[15]Ya. B. Zel'dovich and Yu. P. Raĭzer, Zh. Eksp. Teor. Fiz. **47**, 1150 (1964) [Sov. Phys. JETP **20**, 772 (1965)].
[16]F. V. Bunkin, V. I. Konov, A. M. Prokhorov, and V. B. Fedorov, Pis'ma Zh. Eksp. Teor. Fiz. **9**, 609 (1969) [JETP Lett. **9**, 371 (1969)].
[17]A. I. Barchukov, F. V. Bunkin, V. I. Konov, and A. A. Lyubin, Zh. Eksp. Teor. Fiz. **66**, 965 (1974) [Sov. Phys. JETP **39**, 469 (1974)].
[18]A. N. Pirri, AIAA Paper 76–23 (1976).
[19]P. S. P. Wei and R. B. Hall, J. Appl. Phys. **44**, 2311 (1974).
[20]C. T. Walters, R. H. Barnes, and R. E. Beverly III, J. Appl. Phys. **48**, 2937 (1978).
[21]V. A. Batanov, F. V. Bunkin, A. M. Prokhorov, and V. B. Fedorov, Pis'ma Zh. Eksp. Teor. Fiz. **11**, 113 (1970) [JETP Lett. **11**, 69 (1970)].

[22]B. Steverding, J. Appl. Phys. **45**, 3507 (1974).
[23]V. I. Mazhukin, A. A. Uglov, and B. N. Chetverushkin, Dokl. Akad. Nauk SSSR **246**, 1338 (1979) [Sov. Phys. Dokl. **24**, 443 (1979)].
[24]V. I. Mazhukin, Preprint No. 30 [in Russian], Institute of Applied Mathematics, Academy of Sciences of the USSR, Moscow (1979).
[25]G. W. Sutton and A. Sherman, Engineering Magnetohydrodynamics, McGraw-Hill, New York (1965).
[26]V. I. Mazhukin, A. A. Uglov, and B. N. Chetverushkin, Zh. Vychisl. Mat. Mat. Fiz. **20**, 451 (1980).
[27]I. R. Hurle, in: Low-Temperature Plasma [Russian translation], Mir, Moscow (1967).
[28]A. V. Bondarenko, V. S. Golubev, E. V. Dan'shchikov, F. V. Lebedev, A. F. Nastoyashchiĭ, and A. V. Ryazanov, Pis'ma Zh. Tekh. Fiz. **5**, 221 (1979) [Sov. Tech. Phys. Lett. **5**, 87 (1979)].
[29]A. F. Nastoyashchiĭ, Kvantovaya Elektron. (Moscow) **7**, 170 (1980) [Sov. J. Quantum Electron. **10**, 95 (1980)].
[30]S. A. Losev and G. D. Smekhov, Teplofiz. Vys. Temp. **7**, 1015 (1969).
[31]B. M. Smirnov, Ions and Excited Atoms in Plasmas [in Russian], Atomizdat, Moscow (1974).

Translated by R. M. Durham

Optimization of laser amplifiers with spatial filtering. IV. Deformation of pulses in laser amplifiers

V. V. Lyubimov and L. V. Nosova

(Submitted May 7, 1981)
Kvantovaya Elektron. (Moscow) **9**, 917–924 (May 1982)

Gain diagrams are used to study pulse deformation which must be allowed for in the case of series connection of amplifying stages. The concept of an effective pulse duration is introduced. This concept is used to estimate the maximum breakup integral and to determine the optimal parameters of series-connected amplifying stages in the case when the breakup integral is constant for each stage.

PACS numbers: 42.60.He, 42.60.Da, 42.60.Kg, 42.60.Fc

Construction of large facilities for studies of controlled laser fusion[1-3,11] has made it necessary to consider the problem of the efficiency of extraction of the energy stored in the active medium, which requires operation in a nonlinear amplification regime. It is then necessary to allow for the deformation of pulses in amplifying stages[12] because the efficiency of a thermonuclear reaction in a laser plasma is extremely sensitive to the pulse shape.[4] Moreover, allowance for the deformation of the pulse shape (particularly for its broadening) is essential in the case of series connection of amplifying stages in each of which the breakup integral $(2\pi n_2/n\lambda)\int J(l)dl$ should not exceed its permissible value.[3]

We shall use gain diagrams[5] and the method described in Ref. 6 to analyze the deformation of a pulse in an amplifying stage and we shall show that our earlier results[7] can be used to determine the optimal parameters of the whole chain of amplifying stages.

1. MAXIMUM VALUE OF THE BREAKUP INTEGRAL

The breakup integral should not exceed a certain permissible value so as to ensure the absence of small-scale self-focusing in each of amplifying stages connected in series. In the absence of pulse deformation the maximum of the breakup integral is attained at the moment of maximum intensity of the input (and also output) pulse. If deformation occurs, the moments corresponding to the maxima of these three quantities—the intensities of the input and output pulses and of the breakup integral—generally do not coincide.[8,9] The instantaneous value of the quantity $\int J(l,t)dl$, which governs the breakup integral, can be calculated using a formula introduced in Ref. 6:

$$\int J(l,t)\,dl = \frac{J_{\text{in}}(t)}{E_{\text{in}}(t)}\frac{E_{\text{out}}(t)-E_{\text{in}}(t)}{k\eta(E_{\text{in}})-\rho} = \frac{J_{\text{out}}(t)}{E_{\text{out}}(t)}\frac{E_{\text{out}}(t)-E_{\text{in}}(t)}{k\eta(E_{\text{out}})-\rho}, \quad (1)$$

where $J(t)$ is the power density; $E(t)=\int_{-\infty}^{t}J(\tau)d\tau$; $\eta(E)$ is the saturation coefficient[6]; k is the gain of the active medium; ρ represents the losses. In estimating the breakup interval we can usefully introduce the concept of an effective pulse duration $\tau(t)=E(t)/J(t)$, determined at that moment in time when the breakup integral is maximal. The convenience of this definition of the effective pulse duration is related to the fact that the formula deduced earlier[6] for the instantaneous value of the output power density

$$\frac{J_{\text{out}}(t)}{J_{\text{in}}(t)} = \frac{E_{\text{out}}(t)\,[k\eta(E_{\text{out}})-\rho]}{E_{\text{in}}(t)\,[k\eta(E_{\text{in}})-\rho]} \quad (2)$$

determines the change in the effective duration between the input of an amplifying stage and its output:

$$\frac{\tau_{\text{out}}}{\tau_{\text{in}}} = \frac{k\eta(E_{\text{in}}(t^*))-\rho}{k\eta(E_{\text{out}}(t^*))-\rho}, \quad (3)$$

 0049-1748/82/050580-05$04.10 © 1982 American Institute of Physics